© ESO 2011

X-ray spectral properties of Seyfert galaxies and the unification scheme

Veeresh Singh[1,2,⋆], Prajval Shastri[1] and Guido Risaliti[3,4]

[1] Indian Institute of Astrophysics, Bangalore 560034, India
[2] Department of Physics, University of Calicut, Calicut 673635, India
[3] INAF-Osservatorio di Arcetri, Largo E. Fermi 5, I-50125 Firenze, Italy
[4] Harvard-Smithsonian Center for Astrophysics, 60 Garden St. Cambridge, MA 02138, USA

ABSTRACT

Aims. The unification scheme of Seyfert galaxies predicts that the observed differences between type 1 and type 2 Seyfert galaxies are solely due to the differing orientations of the toroidal-shaped obscuring material around AGN. The observed X-ray spectra of Seyfert type 2s compared to type 1s are expected to be affected by higher absorbing column density due to the edge-on view of the obscuring torus. We study the 0.5 - 10 keV X-ray spectral properties of Seyfert type 1s and type 2s with the aim to test the predictions of Seyfert unification scheme in the X-ray regime.

Methods. We use an optically selected Seyfert sample in which type 1s and type 2s have matched distributions in the orientation independent parameters of AGN and host galaxy.

Results. The 0.5 - 10 keV *XMM-Newton* pn X-ray spectra of Seyfert galaxies are in general best fitted with a model consists of an absorbed power-law, a narrow Gaussian fitted to the Fe Kα emission line and an often seen soft excess component characterized by either a thermal plasma model with temperature kT ∼ 0.1 - 1.0 keV and/or a steep power-law. The 2.0 - 10 keV hard X-ray continuum emission in several Seyfert type 2s is reflection dominated and suggests the Compton-thick obscuration. Results on the statistical comparison of the distributions of the observed X-ray luminosities in the soft (0.5 - 2.0 keV) and hard (2.0 - 10.0 keV) bands, the X-ray absorbing column densities, the equivalent widths of Fe Kα line and the flux ratios of hard X-ray to [OIII] λ5007Å for the two Seyfert subtypes are consistent with the obscuration and orientation based unification scheme.

Key words. Galaxies: Seyfert – X-rays: galaxies – Galaxies: active

1. Introduction

Seyfert galaxies are classified mainly into two classes, based on the presence (type 1) or absence (type 2) of broad emission lines in their optical spectra (Antonucci 1993). The unification scheme of Seyfert galaxies hypothesizes that Seyfert type 1s and type 2s constitute the same parent population and appear different solely due to the differing orientations of the AGN axis *w.r.t.* the line-of-sight. The scheme requires the presence of toroidal-shaped dusty molecular obscuring material around the AGN. In the type 2s, this torus is inclined edge-on and blocks the direct view to the nuclear region, while in type 1s the observer's line-of-sight is away from the plane of the torus and the central region is visible (Antonucci & Miller 1985; Antonucci 1993; Urry et al. 1995).

Several investigations in the literature have yielded results consistent with the predictions of this scheme, such as, the presence of broad emission lines in the polarized optical and infrared spectra of many Seyfert 2s (Moran et al. 2000), the biconical structure of the narrow line region (Mulchaey et al. 1996), the similarity of CO masses of the two Seyfert subtypes (Maiolino et al. 1997), and similar nuclear radio properties of both the subtypes (Lal et al. 2011). Inconsistencies with the predictions of the scheme remain however, *e.g.*, the absence of hidden Seyfert 1 nuclei in several Seyfert 2s (Tran 2001, 2003), Seyfert 1s being preferentially hosted in galaxies of earlier Hubble type (Malkan et al. 1998), the lack of X-

ray absorption in some Seyfert 2s (Panessa & Bassani 2002), and Seyfert 2s having a higher propensity for nuclear starbursts (Buchanan et al. 2006). Moreover, it has been evident that the sample selection plays a crucial role in testing the predictions of Seyfert unification scheme (Antonucci 2002). Ho & Ulvestad (2001) have discussed that the optical and UV selected samples are likely to have inherent biases against the obscured sources. IR selected samples can be biased towards unusually dusty as well as sources which have higher level of nuclear star formation (Ho & Ulvestad 2001; Buchanan et al. 2006). X-ray selected samples have also been used to examine the validity of Seyfert unification (Awaki et al. 1991; Smith & Done 1996; Turner et al. 1997a,b, 1998; Bassani et al. 1999). However, the Seyfert samples selected from flux limited surveys are likely to have obscured type 2 Seyferts that are intrinsically more luminous than the selected type 1 counterparts. Maiolino et al. (1998) and Risaliti et al. (1999) have shown the increased number of heavily obscured type 2 sources using a sample based on [OIII] λ5007Å line luminosity, suggesting the generally inherent bias against less luminous and heavily obscured sources in X-ray selected samples. Hard X-ray selected samples are suppose to be less biased but cannot be granted to be free from biases against heavily obscured Compton-thick and low luminosity AGNs (Heckman et al. 2005; Wang et al. 2009). Recent Seyfert samples based on *INTEGRAL* and *Swift*/BAT surveys preferentially contain relatively large number of high luminosity and less absorbed Seyferts (Tueller et al. 2008; Treister et al. 2009; Beckmann et al. 2009), possibly due to less effective area

⋆ veeresh@iiap.res.in

which limits the sensitivity only to ($\sim 10^{-11}$ erg s^{-1} cm^{-2}) bright sources.

The quest of testing the validity and limitations of the Seyfert unification with more improved and well defined samples still continues. Recent studies by Cappi et al. (2006); Dadina (2008); Beckmann et al. (2009) used less biased optically and X-ray selected samples and reported the results broadly consistent with unification, nonetheless, issues related to sample selection still remains. Keeping the above sample selection arguments in mind we opted to use a sample in which the distributions for type 1 and type 2 Seyferts are matched in orientation independent parameters. Such sample selection mitigates the biases generally inherent in flux limited surveys and also ensures that the two Seyfert subtypes are intrinsically similar within the framework of Seyfert unification scheme (Schmitt et al. 2003; Lal et al. 2011).

In the standard picture of the unification scheme, AGN powered by accretion on to supermassive black hole and surrounding broad line region clouds are embedded in an obscuring torus (Antonucci & Miller 1985; Antonucci 1993; Urry et al. 1995). The X-ray emission originating from the AGN carries the imprints of obscuring and reprocessing material. Therefore Seyfert X-ray spectra are expected to differ depending upon whether the AGN is viewed directly (*i.e.*, type 1s) and through the obscuring torus (*i.e.*, type 2s). In Seyfert type 2s, the intrinsic X-ray emission is attenuated by the obscuring torus and the observed flux as well as the X-ray spectral shape depend on the optical depth of the obscuring torus (Awaki et al. 1991; Smith & Done 1996; Turner et al. 1997a; Bassani et al. 1999; Cappi et al. 2006). Since the photoelectric absorption cross-section decreases with the increase in photon energy, an increasing fraction of primary high energy photons are expected to transmit through the torus. Therefore, Seyfert type 1s and type 2s are expected to show systematically less difference for the observed hard X-ray luminosities and more difference for the soft X-ray (E < 2.0 keV) luminosities. Since in type 2s, AGN is viewed through the obscuring torus therefore type 2s are expected to show systematically higher absorbing column densities than type 1s. The absorbing column density can be measured via photoelectric absorption component in 0.5 - 10 keV spectral fits as long as obscuration is Compton-thin ($N_H < 10^{24}$ cm^{-2}). If obscuration is Compton-thick ($N_H > 10^{24}$ cm^{-2}), type 2s become faint even at higher X-ray energies since high energy photons are Compton-down scattered to soft photons which eventually get absorbed or scattered out of the line-of-sight (Matt et al. 2000a). The equivalent width (EW) of Fe Kα line also increases with the absorbing column density as it is measured against much depressed continuum and for Compton-thick sources it increases to $\sim$ 1 keV (Ghisellini et al. 1994; Levenson et al. 2006). The flux ratio of hard X-ray (2.0 - 10 keV) to [OIII] $\lambda5007$Å line emission can also be used as a diagnostic parameter for the amount of obscuration and type 2s compared to type 1s are expected to show lower flux ratios of hard X-ray to [OIII] (Bassani et al. 1999; Cappi et al. 2006). In this paper we test these predictions of the unification scheme by comparing the properties such as the observed soft and hard X-ray luminosities, the X-ray absorbing column densities, the EWs of Fe Kα line and the flux ratios of X-ray to [OIII] $\lambda5007$Å for the Seyfert type 1s and type 2s. In other words, using 0.5 - 10 keV *XMM-Newton* data we test whether X-ray properties conform with the optical classification of Seyfert type 1s and type 2s in the framework of the orientation and obscuration based unification scheme. The important aspect of our study is the sample selection in which type 1s and type 2s are matched in orientation-independent parameters.

A description of the sample, observations and data reduction is given in the section 2 and 3, section 4 describes the spectral modeling of X-ray spectra and the statistical comparisons of X-ray spectral properties of the two Seyfert subtypes have been discussed in section 5. Notes on individual Seyfert galaxies are given in the appendix. In this paper, we assume $H_0 = 71$ km^{-1} Mpc^{-1}, $\Omega_m = 0.27$, and $\Omega_{vac} = 0.73$.

2. The Sample

We use the sample of Lal et al. (2011) which is consist of 20 (10 type 1 and 10 type 2) optically selected Seyfert galaxies. This sample was formulated to study the nuclear radio properties in the framework of Seyfert unification scheme and in this paper we attempt to test the predictions of Seyfert unification scheme in the X-ray regime using the same sample. Although, the sample was formulated to study parsec-scale radio emission and is constrained by VLBI observing feasibility criteria, it is adequately qualified to test the predictions of unification scheme in the X-ray regime since it is based on the orientation-independent parameters. In this sample Seyfert galaxies are defined as radio quiet ($\frac{F_{5 \ GHz}}{F_{B-band}} < 10$) (Kellermann et al. 1989), low optical luminosity AGN ($M_B > $ -23) (Schmidt & Green 1983), hosted in spiral or lenticular galaxies (Weedman 1977). All the intermediate subclasses Seyferts (*i.e.*, 1.0, 1.2, 1.5, 1.8, 1.9) which show any broad permitted emission line component in their optical spectra are grouped as type 1s, while those which show only narrow permitted emission lines are considered as type 2 Seyferts. The sample is selected such that the two Seyfert subtypes have matched distributions in the orientation-independent parameters of AGN and host galaxy and the sources which were deviating in matching the type 1 and type 2 distributions of the orientation-independent parameters were left out. In other words, the sources should lie within the same range of values for a given parameter to enter into the sample. Also, it was ensured that in a given bin of a parameter distribution type 1s do not outnumber the type 2s and vice-versa. Indeed, there is a possibility to increase the sample size following the same sample selection criteria, however, we would like to emphasize that the more important is the sample selection criteria and not the sample size to rigorously test the predictions of the unification scheme. Larger but heterogeneous and biased sample is likely to result incorrect conclusions.

Cosmological redshift, [OIII] $\lambda5007$Å line luminosity, Hubble stage of the host galaxy, absolute stellar magnitude of the host galaxy and absolute magnitude of the bulge are considered as the orientation-independent properties for the sample selection. These properties do not depend on the orientation of the obscuring torus, AGN axis and the host galaxy. And, indeed all these properties are intimately linked to the evolution of AGN as well as host galaxy. We refer reader to see Lal et al. (2011) for the detailed description on the sample selection and on the matching of the distributions of the orientation-independent parameters for the two Seyfert subtypes. The matching of type 1s and type 2s in orientation-independent isotropic parameters ensures that we are not comparing entirely intrinsically different sources selected from different parts of the (luminosity, bulge mass, Hubble type, redshift) evolution function.

3. X-ray observations and data reduction

We modeled the X-ray spectra of our sample sources using *XMM-Newton* EPIC-pn observations obtained from *XMM-*

Table 1. *XMM-Newton* EPIC pn observations log

Source name	Obs. mode/filter	Obs. date	Obs. time (ks)	Net expo. time (ks)	ct/s	Obs. ID	R_S (arcsec)
MCG+8-11-11	SW/Medium	2004-04-10	38.45	25.24	14.93	0201930201	35.0
MRK 1218	SW/Thin	2005-04-09	13.87	6.55	0.53	0302260201	20.0
NGC 2639	FW/Thin	2005-04-03	26.12	4.23	0.24	0301651101	16.0
NGC 4151	SW/Medium	2006-11-29	52.81	24.60	9.57	0402660201	40.0
MRK 766	SW/Medium	2005-05-24	95.51	60.12	4.92	0304030101	40.0
MRK 231	FW/ Medium	2001-06-07	22.34	17.30	0.10	0081340201	30.0
ARK 564	SW/Medium	2005-01-06	101.77	69.07	39.67	0206400101	35.0
NGC 7469	SW/Medium	2004-12-03	79.11	54.95	21.59	0207090201	37.5
MRK 926	SW/Thin	2000-12-01	11.76	7.19	18.33	0109130701	37.5
MRK 530	SW/Thick	2006-06-14	16.82	11.42	12.93	0305600601	20.0
MRK 348	FW/Medium	2002-07-18	49.50	26.54	1.96	0067540201	22.5
MRK 1	FW/Thin	2004-01-09	11.91	8.66	0.07	0200430301	17.5
NGC 2273	FW/Medium	2003-09-05	13.02	5.21	0.08	0140951001	20.0
MRK 78	FW/Thin	2006-03-11	16.12	4.83	0.09	0307001501	22.5
NGC 7212	FW/Thin	2004-05-20	14.22	10.50	0.10	0200430201	20.0
MRK 533	LW/Thick	2004-06-02	10.42	7.51	0.12	0200660101	17.5
NGC 7682	FW/Thin	2005-05-27	20.21	14.27	0.04	0301150501	16.0

Notes: SW: Small Window, FW: Full Window, LW: Large Window, R_S: radius of the circular region around the source used for spectral extraction.

Newton Science Archive. High throughput (especially, at energies E ≥ 2.0 keV) of *XMM-Newton* allows to search for spectral components with absorbing column density up to $N_H \sim 10^{24}$ cm^{-2} and its good spatial resolution minimizes any strong contamination from off-nuclear X-ray emission. For our X-ray spectral study, we use only EPIC pn data and did not include EPIC MOS data since it is more susceptible to pile-up for bright X-ray sources and few sources, *e.g.*, MRK 530 do not have MOS data. Also, EPIC pn data is good enough for our purpose of obtaining the average X-ray spectral parameters (*e.g.*, photon index, equivalent hydrogen column density, EW of Fe Kα emission line) of our sample sources. In case of a source had more than one observations in archive, we chose the latest one with sufficient long exposure time. The observation log is given in table 1 and gives the details of observing modes of pn camera, used optical light blocking filters, observation dates, observation and net exposure times, count rates, observation IDs and radius (in arcsec) of the circular region around the source position used to extract the X-ray spectra. The raw observation data files (ODFs) were reduced and analyzed using the standard Science Analysis System (SAS) software package (version 7.1) with the latest calibration files. The time intervals of high energy background particle flares were removed by applying fixed threshold on single events, using E ≥ 10.0 keV, and δt = 50 sec light curves. The background is extracted from a circular region in the same chip. In order to apply χ^2 statistics the spectra were binned with minimum 20 counts per bin.

We present the X-ray spectra of 17 (10 type 1s and 7 type 2s) out of 20 Seyfert galaxies of the sample using *XMM-Newton* pn archival data. For 6 Seyfert galaxies, *i.e.*, MRK 1218, NGC 2639, MRK 530, MRK 78, MRK 533 and NGC 7682, the *XMM-Newton* X-ray spectra are presented for the first time and for two Seyferts, *i.e.*, NGC 4151 and NGC 7469, the *XMM-Newton* archival data chosen by us have not been published. The *XMM-Newton* spectra of rest of the 9 sources have been individually published, however, to have uniform reduction and analysis, we re-do the X-ray spectral fitting of these sources using data reduced with most updated calibration files. Also, a priori we do not rule out the possibility of obtaining the different or better fits for these 9 sources and therefore we prefer to re-do the spectral analysis for these sources. For 3 (type 2) Seyfert galaxies of

our sample, *i.e.*, NGC 5135, MRK 477 and NGC 5929, there are no *XMM-Newton* data and we are using *Chandra* and *ASCA* spectral parameters for these sources from literature while performing the statistical comparison of the X-ray properties of the two subtypes of Seyferts.

4. X-ray spectral analysis

We attempt to obtain the physically motivated best fits for the 0.5 - 10.0 keV *XMM-Newton* pn X-ray spectra of our sample Seyfert galaxies. Since the primary aim of spectral analysis is to identify the underlying continuum components, we first tried to fit each spectrum with a simplest model consists of a power-law plus absorption fixed at the Galactic value plus intrinsic absorption as a free parameter. However, in most of the cases this simple parametrization is insufficient to model the whole spectrum and residuals often show a soft excess and an emission line feature at 6.4 keV on top of the (absorbed or unabsorbed) power-law. In most of the cases, we found the best fit model consists of a power-law with a photoelectric cutoff due to cold absorption from the Galactic column density and neutral gas at the redshift of the source; a narrow Gaussian line to reproduce the iron Kα fluorescent emission line at 6.4 keV in the rest frame with energy, width and intensity as free parameters; soft excess component characterized by either a steep power-law and/or a thermal plasma model with temperature kT. In some cases reflection component characterized by reflection from an isotropically illuminated cold slab (model PEXRAV (Magdziarz & Zdziarski 1995) in XSPEC (Arnaud 1996)) is required for the best fit. A partial covering of the primary power-law component is also needed for the best fit in some sources. The partial covering model is equivalent to a combination of an absorbed power-law plus a scattered power-law, assuming that the power-law slopes of these two components are same. We note that for many of our sample sources, the 0.5 - 10.0 keV X-ray spectra can approximately be modeled as "exp(-N_{H_0} σ_{abs}) × [soft component + exp(-N_{H_1} σ_{abs}) (AE$^\Gamma$ + emission lines)]", as suggested by Nandra & Pounds (1994); Awaki et al. (2000), where N_{H_0} and N_{H_1} are the Galactic and source column densities, respectively. Table 2 describes the best fit spectral parameters of all the sample sources and figure 1 shows the best spectral fits of 17 sample

sources. Errors on the spectral fit parameters and derived quantities are at 90% confidence level.

4.1. X-ray spectral components

In the following sections we describe the main components of the 0.5 - 10 keV spectra of our sample Seyfert galaxies.

4.1.1. Absorbed power-law

The X-ray continuum of Seyfert galaxies can primarily be characterized by a photoelectric absorbed power-law. Figure 3 shows the distributions of equivalent hydrogen column density for the two subtypes of Seyferts of our sample. The estimated column densities in Seyfert galaxies of our sample varies from Galactic value to as high as the limiting value of Compton-thick obscuration ($N_H \geq 1.5 \times 10^{24}$ cm^{-2}). As expected in the unification scheme, Seyfert type 1s of our sample are systematically less absorbed than type 2s.

Among type 2s, many sources (*e.g.*, MRK 1, NGC 2273, MRK 78, NGC 5135, NGC 7212, MRK 533 and NGC 7682) are heavily obscured and show only the reflection component in the 2.0 - 10 keV band. We identify these 7 type 2 Seyferts as Compton-thick sources with equivalent hydrogen column density along the line-of-sight 1.5×10^{24} cm^{-2} or higher and exhibiting reflection dominated spectra in the 2.0 - 10.0 keV band. The hard (2.0 - 10.0 keV) component of all the Seyfert type 1s is fitted with an absorbed power-law and our best fits render photon indices (Γ) ~ 1.5 - 2.5 with the mean value of ~ 2.0, while type 2s have either similar hard X-ray photon indices with high absorption or only pure reflection component. In the cases, where both direct as well as reflection components are considered, we fix the reflection component photon index equal to that of the direct power-law component. In some cases equally good fits can be obtained either using unabsorbed or less absorbed flat (Γ ~ 0.5 - 1.0) power-law or with relatively more absorbed steep (Γ ~ 1.8 - 2.1) power-law. In such cases we preferred the more absorbed steep power-law fit as the power-law photon index is closer to the canonical value for Seyfert galaxies (Cappi et al. 2006). We do not perform the statistical comparison of the photon indices of the two Seyfert subtypes since in many of the type 2 sources, the 2.0 - 10.0 keV hard X-ray spectrum is best fitted by pure reflection component and without the presence of any transmitted power-law component from AGN. Therefore in such reflection dominated sources we do not have the photon index of the direct power-law component.

4.1.2. Soft X-ray excess

17 among the 20 Seyferts of our sample exhibit the soft excess, *i.e.*, emission above the extrapolation of the absorbed AGN power-law. 3 (type 1) sources, *i.e.*, MCG+8-11-11, MRK 1218 and MRK 926 do not show any presence of the soft excess. We fit the soft excess by a thermal plasma model MEKAL (Mewe-Kaastra-Liedahl (1995)) and/or by a steep power-law. The typical temperature of the thermal plasma corresponds to kT $\simeq$ 0.1 - 1.0 keV and the soft X-ray photon index is typically 2.5 - 3.5, however, in two cases (MRK 78, NGC 7682) the best fit photon index is as steep as ~ 7.0 and 5.4, respectively. In some cases (*e.g.*, NGC 4151, MRK 766 and NGC 7212), we see emission line features in 0.5 - 2.0 keV part of the spectrum, which indicates the presence of a sub-keV thermal plasma.

The origin of soft excess can be attributed to circumnuclear gas heated to million degrees by shocks induced by AGN outflows (King 2005), an intense circumnuclear star formation (Cid Fernandes et al. 1998; González Delgado et al. 2001) or the photoionization and photoexcitation of circumnuclear gas by the primary AGN emission. Recent high-resolution spectra of few sources, *e.g.*, NGC 1068 (Young et al. 2001; Kinkhabwala et al. 2002), the Circinus galaxy (Sambruna et al. 2001), MRK 3 (Sako et al. 2000; Bianchi et al. 2005b; Pounds & Page 2005); NGC 4151 (Schurch et al. 2004) have provided evidence that the soft excess is largely due to circumnuclear gas photoionized by primary AGN emission. Using a large sample of type 1 AGNs, Mateos et al. (2010) noticed the presence soft X-ray excess in a substantial fraction of nearby sources and fitted it with a thermal plasma model with mean rest-frame temperature kT ~ 100 eV. Mateos et al. (2010) ruled out the origin of the soft excess as thermal emission from the accretion disk or Compton scattered disk emission on the basis of the temperatures detected and the lack of correlation of the soft excess temperature with the hard X-ray luminosity.

4.1.3. Reflection component

Previous X-ray spectral studies reported that many Seyferts, in particular type 2s, show the presence of a reflection component (Awaki et al. 2000). Compton reflection of nuclear radiation from optically thick material can be an important component in Seyfert type 2s and beside absorption, a flat spectrum can result from Compton reflection component (Matt et al. 1996). In highly obscured ($N_H \geq 1.5 \times 10^{24}$ cm^{-2}), *i.e.*, Compton-thick sources, the primary radiation is almost completely absorbed (at E $\leq$ 10 keV), but these sources are still observable through the reflected radiation. There are 7 type 2 sources in our sample in which the 2.0 - 10.0 keV part of the spectrum is best fitted with reflection component alone (PEXRAV model in XSPEC; Magdziarz & Zdziarski (1995)). The large EW of Fe Kα line in these sources is consistent with the Compton-thick obscuration and reflection-dominated spectrum (Ghiselini et al. 1994; Levenson et al. 2006). Some type 1 sources, *e.g.*, MCG+8-11-11, NGC 4151, MRK 766 and MRK 926 also show the presence of a reflection component at the hard end of the spectrum. This can be expected in the framework of the unification scheme since a similar obscuring material having toroidal geometry is present but the plane of the torus lies away from the line-of-sight and thus the reflection component is much fainter in compared to the direct transmitted component. Moreover, at the hard end of the spectrum (E $\geq$ 8.0 keV) the reflection component may have significant contribution.

4.1.4. Fe K$_\alpha$ and other emission lines

We detected fluorescent Fe Kα emission line at ~ 6.4 keV in all (except NGC 2639) of our sample sources suggesting the ubiquitous presence of Fe Kα line in the X-ray spectra of Seyfert galaxies. In most of the sources the centroid energy of Fe Kα emission line is consistent with the emission from neutral or mildly ionized iron. In some sources, *e.g.*, MRK 766, MRK 231, ARK 564, MRK 533 and NGC 7682, an emission line at ~ 6.7 - 7.1 keV is also present, which is possibly either H or He like ionized Fe Kα line component or a neutral component of Fe K$_\beta$ emission line. When the absorbing column density increases to a few times of 10^{23} cm^{-2}, the equivalent width of Fe Kα increases, since it is measured against a depressed continuum. The

equivalent width can be higher than 1.0 keV for column densities of $N_H \geq 10^{24}$ cm^{-2}, and such values are indeed observed in heavily absorbed and Compton-thick sources (Maiolino et al. 1998). Figure 3 shows the distributions of EWs of Fe Kα line for the two subtypes of Seyferts of our sample. Seyfert type 1s have EWs $\sim$ 20 - 250 eV while for type 2s (except MRK 348) it ranges from $\sim$ 0.5 keV to $\sim$ 2.0 keV. High EWs of Fe Kα line in type 2s suggests high obscuration compared to type 1s.

Apart from the ubiquitous Fe Kα emission line we also notice the presence of other emission lines in some of our sample sources, mainly in the soft X-ray band. The addition of Gaussian emission line at $\sim$ 0.88 keV in NGC 4151 and NGC 7212 improves the fit and is likely to be associated with O VIII radiative recombination continua (Griffiths et al. 1998). High resolution spectroscopic observations show that the soft X-ray emission in NGC 4151 is dominated by X-ray emission lines and radiative recombination continua (RRC) from hydrogen-like and helium-like ionization states of neon, oxygen, nitrogen and carbon (Schurch et al. 2004). Also, in MRK 766 the addition of Gaussian emission feature at $\sim$ 0.5 keV improves the fit and may arise due to the blending of few narrow emission lines.

5. Comparison of the X-ray spectral properties of the two Seyfert subtypes

In this section we discuss the statistical comparison of the distributions of X-ray luminosities and spectral properties of the two subtypes of Seyferts in the framework of Seyfert unification scheme.

5.1. Soft (0.5 - 2.0 keV) and hard (2.0 - 10.0 keV) band X-ray luminosities

Table 5 lists the fluxes, luminosities in the soft (0.5 - 2.0 keV) as well as hard (2.0 - 10.0 keV) X-ray bands and the flux ratios of the hard X-ray to [OIII] λ5007Å line emission. Figure 2 shows the X-ray luminosity distributions for the two Seyfert subtypes in the soft (0.5 - 2.0 keV) as well as hard (2.0 - 10.0 keV) X-ray bands. The observed soft X-ray luminosities for Seyfert type 1s in our sample range from $\sim 10^{40}$ erg s^{-1} to $\sim 10^{44}$ erg s^{-1} with the median value $\sim 6.58 \times 10^{42}$ erg s^{-1}, while for Seyfert type 2s it range from $\sim 10^{38}$ erg s^{-1} to $\sim 10^{42}$ erg s^{-1} with the median value $\sim 6.9 \times 10^{40}$ erg s^{-1}. The two sample Kolmogorov - Smirnov test shows that the soft (0.5 - 2.0 keV) X-ray luminosity distributions of type 1 and type 2 Seyferts are completely different, *i.e.*, null hypothesis that two distributions are same is rejected at 99% level of significance. Seyfert type 2s have systematically lower soft X-ray luminosities than type 1s. The nearly 2 Dex difference in the medians of the soft X-ray luminosities of two Seyfert subtypes can be explained as the presence of more line-of-sight obscuration in type 2s than that in type 1s, which is expected since torus intercepts observer's line-of-sight according to the orientation based Seyfert unification. In hard X-ray (2.0 - 10.0 keV) band, Seyfert 1s of our sample have luminosities ranging from $\sim 10^{40}$ erg s^{-1} to $\sim 10^{45}$ erg s^{-1} with the median value $\sim 1.1 \times 10^{43}$ erg s^{-1}, while for Seyfert 2s it range from $\sim 10^{40}$ erg s^{-1} to $\sim 10^{44}$ erg s^{-1} with the median value $\sim 6.8 \times 10^{41}$ erg s^{-1}. The difference in the hard X-ray luminosity distributions of the two Seyfert subtypes is lower compared to the soft band and can be explained as hard X-ray (2.0 - 10.0 keV) photons suffer less absorption. According to the unification model, at sufficiently high energy one can expect similar X-ray luminosities for the two Seyfert subtypes as the torus op-

tical thickness decreases with the increase in photon energy and similar central engines are at work in both subtypes. The substantial difference in the hard X-ray (2.0 - 10.0 keV) luminosity distributions of the two Seyfert subtypes can be understood as due to high absorption in type 2s. We have several heavily obscured (Compton-thick) type 2 sources in our sample in which X-ray continuum below 10.0 keV is completely suppressed and dominated by reprocessed components.

5.2. Line-of-sight obscuration

The cold matter present in between observer and the AGN (consisting of the Galactic and the material at the redshift of AGN) preferentially absorbs soft X-ray from AGN. The photoelectric absorption component in the X-ray spectral modeling renders the amount of absorption along the line-of-sight in terms of the equivalent hydrogen column density, as long as direct transmitted component is seen. In general, we fit the X-ray continuum with a photoelectric absorbed power-law keeping column density and power-law photon index as free parameters and also all the spectral components are at least absorbed by the Galactic equivalent hydrogen column density. Figure shows the distributions of cumulative N_H for the two Seyfert subtypes. The estimated absorbing equivalent hydrogen column densities for our sample sources varies from as low as to Galactic value ($N_H \simeq 10^{20}$ cm^{-2}) to as high as to the Compton-thick value ($N_H \geq 10^{24}$ cm^{-2}). For type 1s the equivalent N_H ranges from $\sim 10^{20}$ cm^{-2} (Galactic value) to $\sim 10^{22}$ cm^{-2} with median value $\sim 10^{21}$ cm^{-2}, while for type 2s it ranges from $\sim 10^{22}$ cm^{-2} to $\geq 10^{24}$ cm^{-2} with median value $\geq 10^{24}$ cm^{-2}. We have $\sim$ 7/10 reflection dominated type 2 sources in which the 2.0 - 10.0 keV hard component is accounted by pure reflection component (PEXRAV model) and therefore we do have only upper limit of N_H values ($\geq 1.5 \times 10^{24}$) in such cases. Seyfert type 2s have systematically higher absorbing column densities than types 1s and the distributions of the absorbing column densities (N_H) are consistent with the orientation based unification scheme. In our small sample we do not find any unobscured type 2 Seyfert, although some previous studies reported the presence of 10% - 30% of unobscured type 2 Seyferts (Panessa & Bassani 2002). While comparing the amount of obscuration for the two Seyfert subtypes we consider only cold absorption accounted by the photoelectric absorption component. In several sources we require partial covering of primary AGN radiation. The best fit values of covering fraction and absorbing equivalent hydrogen column density are mentioned in table 3. In four Seyfert type 1s, *i.e.*, MRK 1218, NGC 4151, MRK 766 and NGC 7469, warm absorption characterized by the ABSORI model (ionized absorber) is needed for the best fit. While using the ABSORI model we fixed the photon index of the power-law of the absori component equal to the photon index of the primary power-law component and the temperature was fixed to 3×10^4 K. The best fit parameter values for N_H and ionization parameters (ξ) are mentioned in table 4. The ionization parameter indicates the ionization state of absorbing material and is defined as $\xi = \frac{L}{nr^2}$, where L is the source luminosity (in $\sim$13.6 eV - 13.6 keV), n is the absorbing gas density and r is the distance of absorber from the ionizing source (see; Osterbrock & Ferland (2006)). The estimated ionization parameter reveals low ionizing material in MRK 1218, NGC 4151 and MRK 766, however, in NGC 7469, the ionization level is high. Using *XMM-Newton* RGS data, Blustin et al. (2007) reported that NGC 7469 shows the evidence of ionized outflowing material with a wide range of ionization (log $\xi \sim$ 0.5 - 3.5).

Table 2. The best fit spectral parameters

Source	Model	N_H $(10^{20}\ cm^{-2})$	Γ_{SX}	kT (keV)	$N_{H,hard}$ $(10^{22}\ cm^{-2})$	Γ_{HX}	$E_{c,rest}$ (keV)	I_{line}	EW (eV)	χ^2/dof
MCG+8-11-11	pha(PL+R+L)	$18.30^{+0.40}_{-0.43}$				$1.84^{+0.02}_{-0.02}$	$6.44^{+0.01}_{-0.01}$	4.95	$97.9^{+10.4}_{-18.5}$	0.99
MRK 1218	pha(abs*PL+L)	$15.20^{+4.30}_{-13.00}$				$1.48^{+0.11}_{-0.17}$	$6.32^{+0.22}_{-0.49}$	0.19	$63.9^{+46.5}_{-52.4}$	0.99
NGC 2639	pha(T+PL)	$16.20^{+17.60}_{-15.60}$		$0.63^{+0.12}_{-0.09}$		$2.21^{+1.83}_{-1.02}$				0.82
NGC 4151	pha(T+PL+pha*abs*pcf*PL+R+L+L)	$6.33^{+3.30}_{-2.60}$	$3.14^{+0.25}_{-0.06}$	$0.13^{+0.01}_{-0.01}$	$0.12^{+0.08}_{-0.03}$	$1.75^{+0.06}_{-0.03}$	$6.39^{+0.01}_{-0.01}$	14.43	$108.4^{+6.5}_{-6.7}$	1.12
							$0.88^{+0.01}_{-0.01}$	1.12	$60.1^{+29.0}_{-4.4}$	
MRK 766	pha(T+abs*pcf*PL+R+L+L+L)	1.35^f		$0.20^{+0.01}_{-0.01}$		$2.17^{+0.10}_{-0.08}$	$6.44^{+0.03}_{-0.03}$	0.50	$47.9^{+13.9}_{-13.5}$	1.09
							$6.67^{+0.06}_{-0.07}$	0.22	$19.3^{+12.6}_{-12.2}$	
							$0.48^{+0.01}_{-0.01}$	5.38	$137.3^{+45.6}_{-37.5}$	
MRK 231	pha(T+T+pcf*pha*PL+L+L)	1.25^f		$0.33^{+0.04}_{-0.03}$	$0.46^{+0.14}_{-0.16}$	$1.57^{+0.14}_{-0.30}$	$6.28^{+0.13}_{-0.13}$	0.16	$215.0^{+123.1}_{-128.1}$	1.04
				$0.99^{+0.14}_{-0.15}$			$6.66^{+0.07}_{-0.20}$	0.15	$243.5^{+167.8}_{-163.5}$	
ARK 564	pha(T+PL+pcf*PL+L+L)	6.38^f	$3.42^{+0.13}_{-0.12}$	$0.97^{+0.04}_{-0.04}$		$2.32^{+0.08}_{-0.10}$	$6.33^{+0.05}_{-0.05}$	0.29	$20.9^{+10.4}_{-9.9}$	1.09
							$6.71^{+0.04}_{-0.03}$	0.41	$32.3^{+11.4}_{-11.5}$	
NGC 7469	pha(T+abs*pcf*PL+L)	4.96^f		$0.18^{+0.01}_{-0.01}$		$2.04^{+0.02}_{-0.02}$	$6.41^{+0.01}_{-0.02}$	2.03	$64.2^{+7.5}_{-9.5}$	1.09
MRK 926	pha(pcf*PL+R+L)	3.59^f				$1.98^{+0.03}_{-0.02}$	$6.33^{+0.06}_{-0.06}$	1.24	$29.1^{+17.3}_{-23.8}$	0.96
MRK 530	pha(T+pcf*PL+L)	4.06^f		$0.20^{+0.02}_{-0.02}$		$2.28^{+0.03}_{-0.01}$	$6.40^{+0.05}_{-0.05}$	1.49	$47.2^{+7.4}_{-8.2}$	1.09
MRK 348	pha(PL+pha*pcf*PL+L)	5.91^f	$2.75^{+0.17}_{-0.16}$		$6.86^{+0.84}_{-1.01}$	$1.70^{+0.07}_{-0.06}$	$6.40^{+0.04}_{-0.04}$	1.59	$34.2^{+10.8}_{-10.4}$	1.05
MRK 1	pha(T+PL+R+L)	5.31^f	$2.55^{+0.30}_{-0.29}$	$0.82^{+0.09}_{-0.10}$	>150	2.0^fR	$6.77^{+0.08}_{-0.09}$	0.01	$1249.2^{+1299.4}_{-857.5}$	0.99
NGC 2273	pha(PL+R+L)	$7.75^{+36.20}_{-7.70}$	$2.79^{+1.87}_{-0.82}$		>150	$0.67^{+0.37}_{-0.92}$R	$6.40^{+0.03}_{-0.02}$	2.74	$2189.2^{+446.2}_{-441.7}$	0.97
MRK 78	pha(PL+R+L)	$65.38^{+30.02}_{-24.48}$	$7.05^{+1.89}_{-1.84}$		>150	$1.01^{+0.44}_{-0.54}$R	$6.37^{+0.05}_{-0.09}$	0.56	$673.0^{+402.9}_{-389.2}$	0.85
NGC 5135^g	pha(T+T+pha*PL+L)	4.58^f		0.08	>150	1.5	6.40	0.52	$1700.0^{+600.0}_{-800.0}$	....
				0.39			1.78	....	....	
MRK 477^l	pha(pha*PL+L)	1.30^f			$24.0^{+17.0}_{-12.0}$	1.9^f	$6.40^{+0.21}_{-0.23}$	....	$560.0^{+560.0}_{-500.0}$	0.35
NGC 5929^c	pha(PL+pha*PL+L)	51.60	1.7		27.7	1.7	6.40	....	350.0	....
NGC 7212	pha(PL+L+L)	5.41^f	$2.32^{+0.23}_{-0.20}$		>150	$0.99^{+0.54}_{-0.37}$R	$6.42^{+0.04}_{-0.04}$	0.74	$712.3^{+256.0}_{-133.4}$	1.15
							$0.89^{+0.04}_{-0.04}$	0.04	$59.6^{+43.1}_{-38.5}$	
MRK 533	pha(T+PL+R+L+L)	5.16^f	$3.75^{+1.45}_{-0.61}$	$0.76^{+0.13}_{-0.10}$	>150	$2.12^{+0.49}_{-0.51}$R	$6.40^{+0.04}_{-0.05}$	0.55	$557.2^{+241.2}_{-292.7}$	0.97
							$7.04^{+0.06}_{-0.04}$	0.53	$665.6^{+387.9}_{-333.7}$	
NGC 7682	pha(T+R+L+L)	$34.88^{+57.82}_{-25.11}$	$5.36^{+2.78}_{-2.38}$		>150	$1.77^{+0.58}_{-0.61}$R	$6.43^{+0.18}_{-0.06}$	0.20	$477.5^{+312.3}_{-310.9}$	0.81
							$7.11^{+0.39}_{-0.09}$	0.13	$457.6^{+460.3}_{-402.9}$	

f: fixed; s: soft component; pha: photoelectric absorption; PL: power-law; L: Emission line fitted with a Gaussian; T: Thermal emission from hot gas (MEKAL model in XSPEC); abs: Ionized absorber (ABSORI model in XSPEC); R: Reflection from cold neutral material (PEXRAV model in XSPEC); pcf: partial covering.

g: Guainazzi et al. (2005a); **l**: Levenson et al. (2001); **c**: Cardamone et al. (2007); emission line fluxes (I_{line}) are in units of 10^{-13} ergs cm^{-2} s^{-1}.

Table 3. Summary of partial covering model parameters

Source Name	N_H (10^{22} cm^{-2})	Covering fraction (f)
NGC 4151	$9.06^{+1.27}_{-0.98}$	$0.69^{+0.04}_{-0.05}$
MRK 766	$6.42^{+0.93}_{-0.56}$	$0.51^{+0.02}_{-0.03}$
MRK 231	$8.35^{+4.02}_{-4.64}$	$0.74^{+0.09}_{-0.25}$
ARK 564	$3.09^{+0.52}_{-0.45}$	$0.61^{+0.26}_{-0.15}$
NGC 7469	$35.55^{+9.93}_{-6.77}$	$0.28^{+0.03}_{-0.03}$
MRK 926	$4.35^{+2.86}_{-1.99}$	$0.15^{+0.06}_{-0.06}$
MRK 530	$14.81^{+5.62}_{-4.18}$	$0.27^{+0.27}_{-0.27}$
MRK 348	$10.47^{+0.68}_{-1.00}$	$0.84^{+0.06}_{-0.06}$

Table 4. Summary of ionized absorber parameters

Source Name	N_H (10^{22} cm^{-2})	Ionization parameter (ξ)
MRK 1218	$0.63^{+0.41}_{-0.32}$	$39.60^{+57.40}_{-38.37}$
NGC 4151	$5.08^{+1.45}_{-1.20}$	$0.31^{+0.40}_{-0.28}$
MRK 766	$0.21^{+0.03}_{-0.02}$	$6.61^{+4.67}_{-1.67}$
NGC 7469	$1.06^{+0.42}_{-0.36}$	$1193.19^{+692.30}_{-232.63}$

Table 6. Medians and Kolmogorov - Smirnov two sample tests for the statistical comparison of various distributions of the two Seyfert subtypes

Distribution	Median		D	p-value
	Type 1s	Type 2s		
log $L_{0.5-2.0\ keV}$	42.82	40.84	0.8	2.06×10^{-3}
log $L_{2.0-10.0\ keV}$	43.02	41.83	0.6	5.25×10^{-2}
log N_H	21.02	> 24.18	1.0	9.08×10^{-5}
log EW (eV)	1.81	2.79	0.9	9.30×10^{-4}
log R_x	0.96	-0.66	0.7	1.48×10^{-2}

Kolmogorov - Smirnov two sample test examines the hypothesis that two samples comes from same distribution. D = Sup x |S1(x) - S2(x)| is the maximum difference between the cumulative distributions of two samples S1(x) and S2(x), respectively. p-value is the probability that the null hypothesis, *i.e.*, two samples comes from same distribution, is correct. $R_x = \frac{Flux(2.0 - 10.0\ keV)}{Flux[OIII]}$.

The presence of warm absorber in NGC 4151 and MRK 766 has also been reported in previous studies (Schurch et al. 2004; Mason et al. 2003).

5.3. Equivalent width of Fe Kα line

We detect fluorescent Fe Kα emission line in all but one (NGC 2639) of our sample sources suggesting the ubiquitous presence of Fe Kα line in the X-ray spectra of Seyfert galaxies. In NGC 2639, due to lack of enough counts above 2.0 keV we could not confirm the presence of Fe Kα emission line. However, using *ASCA* observations of NGC 2639, Terashima et al. (2002) reported the presence of Fe Kα line with EW ~ 1.5 - 3.0 keV. We estimate the EW of Fe Kα line with respect to the modeled continuum and find that Seyfert type 2s have systematically larger EWs (~ 350 eV to 2.2 keV, except of MRK 348), with median value ~ 600 eV than that of type 1s (~ 20 - 200 eV) with median value ~ 64.0 eV. Kolmogorov - Smirnov two sample test shows that the distributions of EWs of Fe Kα line of the two Seyfert subtypes are completely different (*cf.*, table 6). Heavily obscured, *i.e.*, Compton-thick sources are characterized by large EW of Fe Kα line (Krolik et al. 1994; Levenson et al. 2006) and therefore we use the large EW (~ 1.0 keV) of Fe Kα line as an indicator of heavy obscuration as it is measured

against much depressed continuum (N_H ~ 10^{23} - 10^{24} cm^{-2}; Leahy & Creighton (1993)) or against pure reflection component (N_H ~ 10^{24} - 10^{25}; Bassani et al. (1999)). However, identifying a source as the Compton-thick only on the basis of large EW of Fe Kα line may not be correct, since a large EW can arise if the ionizing radiation is anisotropic (Ghisellini et al. 1991), or if there is a lag between a drop in the continuum and line emissions, as observed in NGC 2992 by Weaver et al. (1996).

### 5.4. Flux ratio of hard X-ray to [OIII] $\lambda5007$Å

In order to confirm the high obscuration in Seyfert type 2s than in type 1s we use the flux ratio of hard (2.0 - 10.0 keV) X-ray to [OIII] $\lambda5007$Å and the equivalent width of Fe Kα line as diagnostic tools. Bassani et al. (1999) reported that the flux ratio of hard X-ray to [OIII] $\lambda5007$Å can effectively be used in identifying Compton-thin and Compton-thick sources with latter having flux ratio $\leq$ 1. The flux ratio of hard X-ray to [OIII] $\lambda5007$Å can be used as an indicator of the amount of obscuration since [OIII] originates from the NLR region largely unaffected by the torus obscuration and can be considered as the proxy of the intrinsic AGN power since it is produced by photoionization of NLR clouds by the AGN continuum (Yee et al. 1981; Nelson & Whittle 1995). While estimating the flux ratio of hard X-ray to [OIII] $\lambda5007$Å, the latter ones are corrected for the optical reddening whenever Balmer decrement value was available for a source in literature. We have Balmer decrement (H_α/H_β) values and hence, optical reddening corrected [OIII] fluxes for only 16 (6 type 1s and 10 type 2s) sources of our sample. For reddening correction we use the formula given in Bassani et al. (1999), *i.e.*, $F_{[OIII],cor} = F_{[OIII],obs}[(H_\alpha/H_\beta)/(H_\alpha/H_\beta S)_0]^{2.94}$, where intrinsic Balmer decrement $(H_\alpha/H_\beta)_0$ is assumed 3.0, and only narrow components of H_α, H_β are considered.

The statistical comparison of the distributions of the flux ratios of hard X-ray (2.0 - 10.0 keV) to [OIII] for the two Seyfert subtypes again confirms the systematically higher obscuration is type 2s than type 1s (*cf.*, table 6, figure 3). Also, using this flux ratio as an indicator we note that MRK 1, MRK 78, NGC 5135, MRK 477, NGC 7212, MRK 533 and NGC 7682 have Compton-thick obscuration. X-ray spectral properties, *e.g.*, reflection dominated hard X-ray component, low hard X-ray to [OIII] flux ratio and high EW of Fe Kα line implies that ~ 7 - 8 out of 10 type 2 sources of our sample are Compton-thick ($N_H \geq 1.5 \times 10^{24}$ cm^{-2}). Some of our sample sources, *e.g.*, MRK 477 (Bassani et al. 1999), NGC 5135, NGC 7212 (Levenson et al. 2006), NGC 2273 (Awaki et al. 2009) and MRK 533 (Bianchi et al. 2005a) have already been reported as Compton-thick. In our sample we have only one Seyfert subtype 1.8 (MRK 1218) and one subtype 1.9 (NGC 2639) which are included into type 1s and thus even if we include subtypes 1.8, 1.9 into type 2s, the relative fraction of Compton-thick sources remains high ~ 60% (7-8 source out of 12 type 2s).

6. Conclusions

We investigated the 0.5 - 10 keV X-ray spectral properties of a sample of 20 Seyfert galaxies in which the two Seyfert subtypes have matched distributions in orientation independent parameters. we summarize the conclusions of our study as below.

– X-ray spectra of our sample Seyfert galaxies, in general, are best fitted with a model consists of : a power-law with a photoelectric cutoff due to the cold absorption from the Galactic
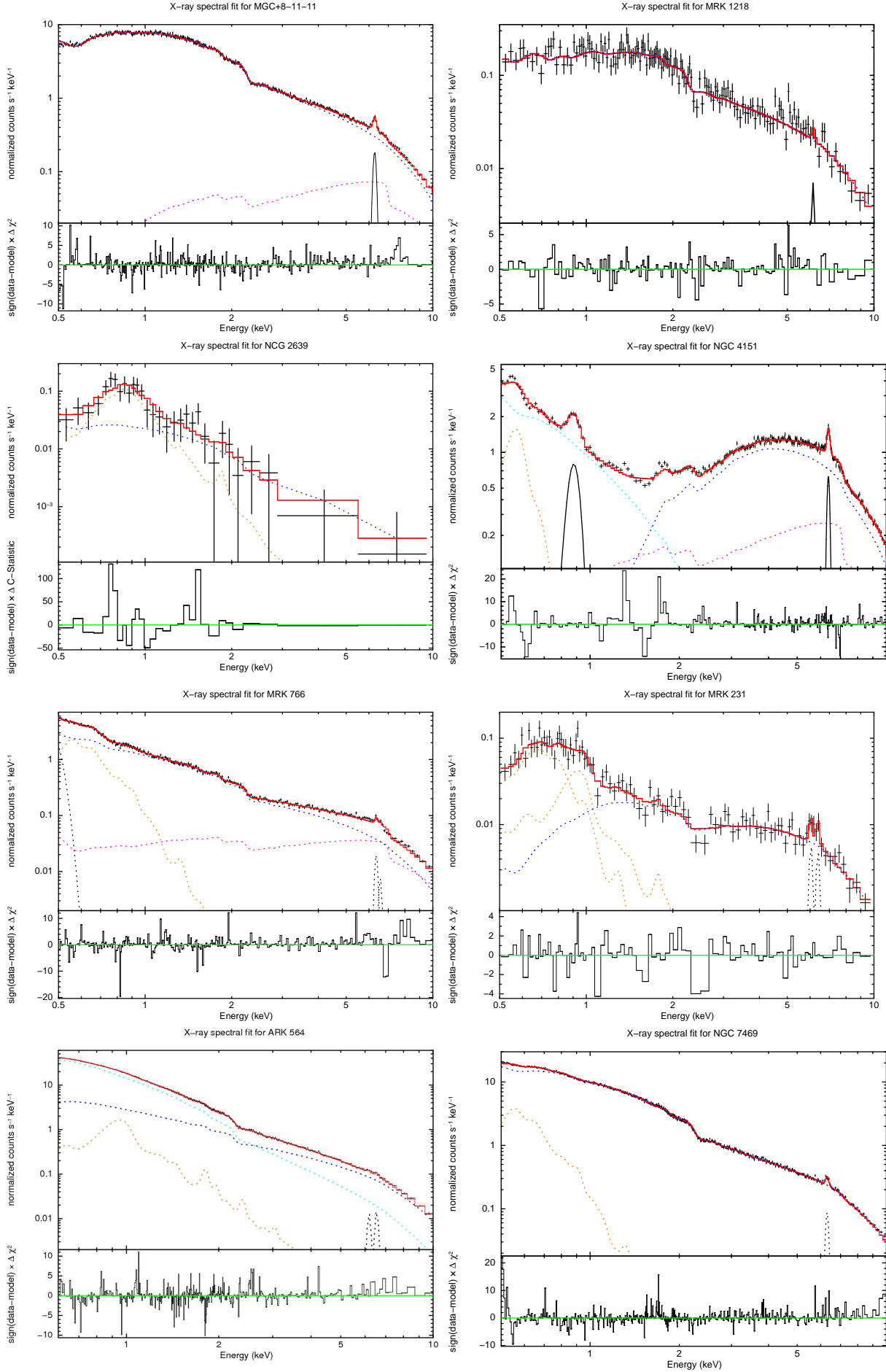
Fig. 1. *XMM-Newton* pn 0.5 - 10.0 keV spectral fits for MCG+8-11-11, MRK 1218, NGC 2639, NGC 4151, MRK 766, MRK 231, ARK 564 and NGC 7469. For each source, top panel shows the cumulative fit (solid curve) along with all the additive spectral components (shown in dotted curves) against the spectral data points and bottom panel shows the residuals.
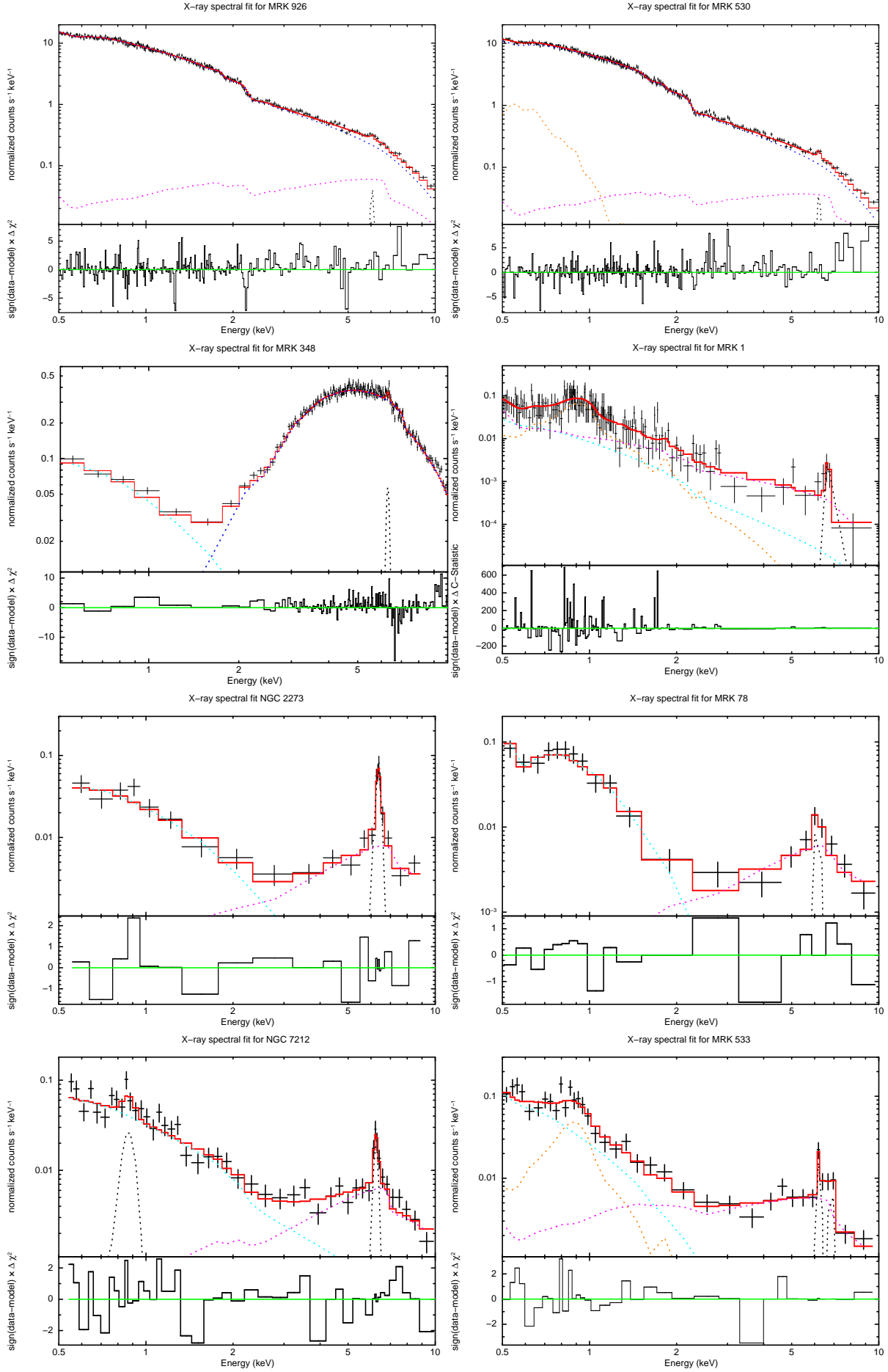
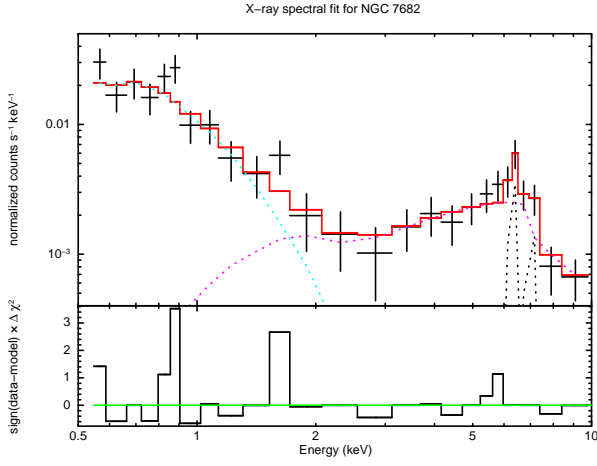**Fig. 1.** continued - spectral fits for MRK 926, MRK 530, MRK 348, MRK 1, NGC 2273, MRK 78, NGC 7212 and MRK 533.

Fig. 1. continued - spectral fit for NGC 7682

Table 5. The observed X-ray fluxes and luminosities in the soft (0.5 - 2.0 keV) and hard (2.0 - 10.0 keV) bands and the flux ratios of hard X-ray to [OIII].

Name	$F_{0.5–2.0\ keV}$	$\log L_{0.5–2.0\ keV}$	$F_{2.0–10\ keV}$	$\log L_{2.0–10\ keV}$	$F^{obs}_{[OIII]}$	Ref.	H_α/H_β	Ref.	$F^{cor}_{[OIII]}$	$\log R_x$
MCG+8-11-11	161.18	43.35	441.97	43.79	6.43	1	4.37	7	19.43	1.36
MRK 1218	4.86	41.96	25.35	42.68	1.70	2	3.26	8	2.17	1.07
NGC 2639	1.26	40.52	0.75	40.29	1.07	3	4.16	9	2.79	-0.57
NGC 4151	29.49	40.75	828.83	42.20	116.00	4	3.1	7	127.74	0.81
MRK 766	33.99	42.10	72.66	42.43	3.95	1	5.1	7	18.79	0.59
MRK 231	0.99	41.60	6.06	42.38	2.30	2	...	...	...	0.42
ARK 564	364.22	43.67	162.25	43.31	1.90	4	...	...	...	1.93
NGC 7469	213.27	43.08	293.41	43.21	5.80	4	9.33	7	162.98	0.26
MRK 926	171.95	43.94	299.05	44.18	3.50	4	...	...	...	1.93
MRK 530	166.48	43.52	182.74	43.56	0.48	4	...	...	...	2.58
MRK 348	1.17	40.76	269.39	43.12	4.12	1	6.02	7	31.93	0.93
MRK 1	0.98	40.74	0.81	40.66	6.00	4	5.89	7	43.61	-1.73
NGC 2273	0.53	39.62	10.02	40.89	1.60	5	6.92	7	18.68	-0.27
MRK 78	0.79	41.39	5.52	42.23	6.60	4	6.46	7	62.93	-1.06
NGC 5135^g	1.90	40.91	1.60	40.83	3.70	6	7.8	9	61.66	-1.59
MRK 477^l	1.20	41.59	12.0	42.59	15.00	4	5.4	7	84.45	-0.85
NGC 5929^c	0.81	40.15	>14.0	>41.39	0.93	4	5.5	7	5.53	>0.40
NGC 7212	0.83	41.13	6.96	42.05	8.75	1	5.01	7	39.52	-0.75
MRK 533	1.42	41.42	6.08	42.06	5.21	1	5.0	7	23.39	-0.59
NGC 7682	0.27	40.22	2.62	41.22	2.30	4	4.8	7	9.16	-0.54

Notes: [OIII] and X-ray fluxes are in unit of 10^{-13} erg cm^{-2} s^{-1}. R_x: $\frac{\text{Flux}(2.0-10.0\ \text{keV})}{\text{Flux[OIII]}}$; **g**: Guainazzi et al. (2005a); **l**: Levenson et al. (2001); **c**: Cardamone et al. (2007). Ref., 1: Schmitt et al. (2003), 2: Dahari & De Robertis (1988), 3: Panessa et al. (2006), 4: Whittle (1992), 5: Ferruit et al. (2000), 6: Polletta et al. (1996), 7: Mulchaey et al. (1994), 8: Dahari & De Robertis (1988), 9: Bassani et al. (1999).

column density and neutral gas at the redshift of the AGN; a narrow Gaussian fitted to the Fe Kα fluorescent emission line at 6.4 keV; often seen soft excess component characterized by either a steep power-law and/or a thermal plasma model with temperature kT ∼ 0.1 - 1.0 keV.

- In several of the heavily obscured type 2 sources, X-ray spectra are completely dominated by reflection component and the hard part of spectra can be characterized with the PEXRAV model and a prominent Fe Kα line.
- Seyfert type 1s have systematically higher observed soft X-ray luminosities than type 2s, as would be expected in the unification scheme with the hypothesis that in type 2s obscuring torus intercepts the AGN view and therefore absorbs the soft X-ray photons emanating from the AGN. The distributions of the observed hard (2.0 - 10 keV) X-ray luminosities of the two subtypes differ much less significantly, consistent with the prediction of unification, as optical thickness

of obscuring material decreases with the increase in X-ray photons energy.

- The X-ray absorbing column density for Seyfert type 1s in our sample ranges from ∼ 10^{20} cm^{-2} (Galactic value) to ∼ 10^{22} cm^{-2} with median value ∼ 10^{21} cm^{-2}, while for type 2s it ranges from ∼ 10^{22} cm^{-2} to Compton-thick limiting value ≥ 10^{24} cm^{-2} with median value ≥ 10^{24} cm^{-2}. The distribution of X-ray absorbing column densities (N_H) for Seyfert galaxies of our sample is broadly consistent with the previous studies (*e.g.*, Cappi et al. (2006); Akylas & Georgantopoulos (2009)).
- Fe Kα fluorescent emission line has been detected in all (except one) of our sample sources suggesting the ubiquitous presence of Fe Kα line in the X-ray spectra of Seyfert galaxies. The centroid energy ∼ 6.4 keV of the line is consistent with the emission from neutral or mildly ionized iron. The equivalent width of Fe Kα line in type 2s ranges ∼ 350 eV
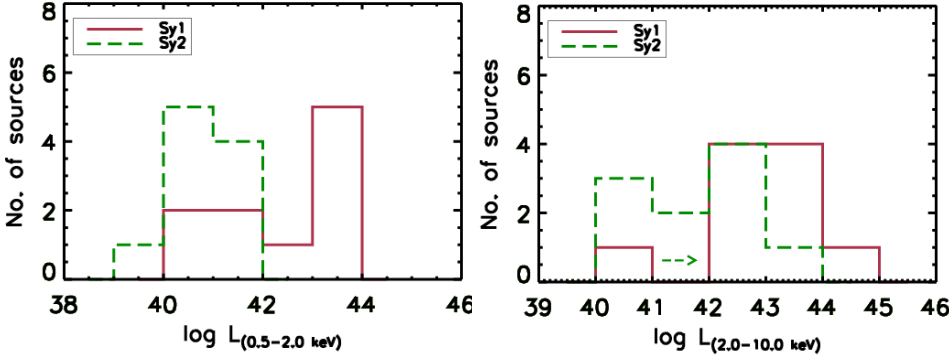
Fig. 2. Distributions of the soft X-ray (0.5 - 2.0) and hard X-ray (2.0 - 10.0) luminosities for the two subtypes of Seyfert galaxies.
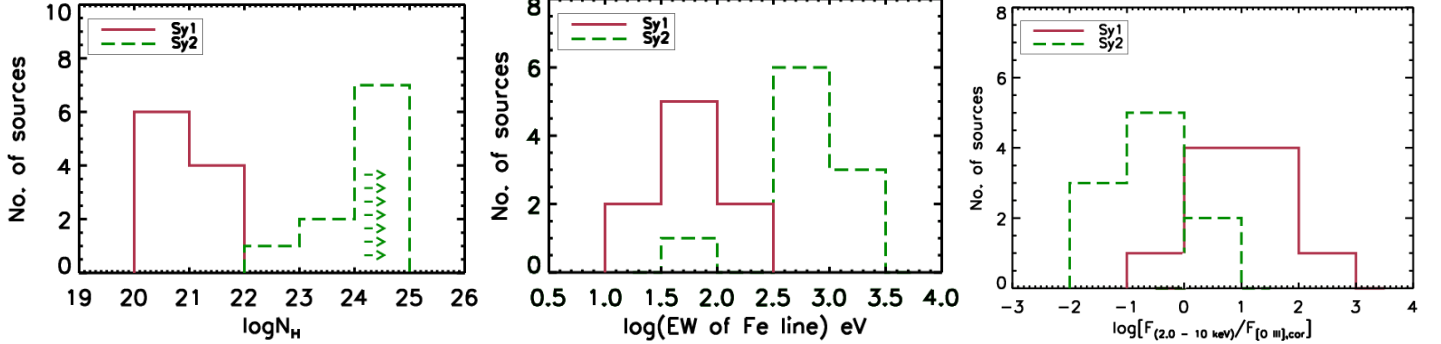

Fig. 3. Distributions of the equivalent hydrogen column density, the equivalent width of Fe Kα and the flux ratio of hard X-ray to [OIII] λ5007Å line for the two subtypes of Seyfert galaxies.

to 2.2 keV and is systematically higher than that of 1s (~ 20 - 200 eV).

– The statistical comparison of X-ray spectral properties, *i.e.*, the X-ray absorbing column densities, the hard X-ray spectral shape (absorbed power-law versus reflection dominated), **the** EWs of Fe Kα line, the flux ratios of hard X-ray to [OIII] λ5007Å, and the luminosity distributions in soft and hard X-ray bands for the two subtypes of Seyfert galaxies are consistent with the orientation and obscuration based Seyfert unification scheme.

– We have argued for the importance of sample selection in testing the Seyfert unification scheme. And, using a sample based on the properties independent to the orientation of the obscuring torus, AGN and host galaxy, we show that the 0.5 - 10 keV X-ray spectral properties are consistent with the unification scheme.

– We also note a high fraction $\sim 70\%$ of heavily absorbed likely to be Compton-thick sources among the type 2 Seyfert population. This high fraction is in agreement with the previous study reported by Risaliti et al. (1999) based on a [OIII] λ5007Å luminosity selected sample of Seyfert 2s and implies that an unbiased sample is essential to estimate the accurate relative fraction of the heavily absorbed, *i.e.*, Compton-thick AGNs. Also, the heavily obscured AGNs may in part responsible for to account missing sources contributing to the Cosmic X-ray background (Worsley et al. 2005; Gilli et al. 2007).

Appendix A: Notes on individual sources

In this section we describe the X-ray spectral properties of individual sources of our sample and the comparison of their X-ray spectral properties with the previous studies.

MCG+8-11-11

MCG+8-11-11 has been observed by all the major X-ray satellites, with the exception of *Chandra*. The *ASCA* (Grandi et al. 1998) and *BeppoSAX* (Perola et al. 2000) data were well fitted by a fairly standard model composed of a power-law, a warm absorber, a Compton reflection component, and an Fe Kα line. Matt et al. (2006) fitted the *XMM-Newton* EPIC pn spectrum with a model composed of an absorbed power-law ($N_H \simeq 1.83^{+0.06}_{-0.03} \times 10^{21}$ cm^{-2}, $\Gamma \simeq 1.805\pm0.015$), a Compton reflection component (with the inclination angle kept fixed to 30°), a Gaussian Fe Kα line (EW $\sim 75\pm15$ eV), warm absorption ($N_{H,warm} \simeq 1.1^{+0.06}_{-0.06} \times 10^{22}$ cm^{-2}) with the temperature of the material fixed at 10^6 K and an absorption edge at 0.74 keV, corresponding to He-like oxygen. Our best fit spectral parameters are broadly consistent with Matt et al. (2006), although we get a good fit without using warm absorption. We also confirm the absence of a soft excess in this source using the *XMM-Newton* EPIC pn data.

MRK 1218

MRK 1218 does not have *Chandra* and *ASCA* observations but has been detected by RoSAT. We present the *XMM-Newton* spectrum of MRK 1218 for the first time. We find that an absorbed power-law ($N_H \simeq 1.52^{+0.43}_{-1.30} \times 10^{21}$ cm^{-2}, $\Gamma \simeq 1.48^{+0.11}_{-0.17}$), with warm absorption ($N_{H,warm} \simeq 0.63^{+0.41}_{-0.32} \times 10^{22}$ cm^{-2}) having plasma temperature fixed at 3×10^4 K and an Fe Kα line of EW $\simeq 63.9$ eV gives the best fit.

NGC 2639

Terashima et al. (2002) fitted the *ASCA* spectrum of NGC 2639 by a partially covered power-law (with $N_{H,1} \sim 0.08$ (≤ 0.32) $\times 10^{22}$ cm^{-2}, $N_{H,2} \sim 32^{+12.5}_{-30} \times 10^{22}$ cm^{-2}, covering fraction $\sim 0.89^{+0.08}_{-0.81}$, $\Gamma \sim 2.8^{+1.0}_{-0.6}$ and $\chi^2/dof \simeq 45.8/49$). They also attempted a model consisting of an absorbed power-law plus a Raymond-Smith (Raymond & Smith 1977) thermal plasma modified by the Galactic absorption. The best fit parameters reported by Terashima et al. (2002) using this model are $N_{H,1} \simeq 0.027 \times 10^{22}$ cm^{-2} (fixed), $kT \simeq 0.80^{+0.27}_{-0.40}$, abundances fixed to 0.5 of solar, $N_{H,2} \sim 0.0$ (≤ 0.31) $\times 10^{22}$ cm^{-2}, $\Gamma \simeq 1.92^{+0.70}_{-0.37}$ and $\chi^2/dof \simeq 45.6/49$. The reported equivalent widths of Fe Kα for these two models are $1.49^{+11.11}_{-1.27}$ keV and $3.13^{+2.27}_{-2.00}$ keV, respectively. We present *XMM-Newton* X-ray spectrum of NGC 2639 first time and find that the best fit consists of an absorbed power-law ($N_H \simeq 1.62^{+1.76}_{-1.56} \times 10^{21}$ cm^{-2}, $\Gamma \simeq 2.21^{+1.83}_{-1.02}$) plus a soft component modeled with a thermal plasma (MEKAL in XSPEC) of temperature $kT \simeq 0.63^{+0.12}_{-0.09}$. We do not detect Fe K$\alpha$ line in the *XMM-Newton* pn spectrum probably due to lack of sufficient counts above 2.0 keV.

NGC 4151

NGC 4151 is one of the most extensively studied Seyfert galaxies in nearly all wavelengths. The *ASCA* and *BeppoSAX* X-ray spectra were fitted with a flat absorbed power-law ($\Gamma \simeq 1.65$), a contribution from a cold reflector and a two-component absorber, an intrinsic neutral component with $N_H \simeq 3.4 \times 10^{22}$ cm^{-2} and a highly ionized absorber with $N_H \simeq 2.4 \times 10^{23}$ cm^{-2} (Schurch & Warwick 2002; Piro et al. 2005). Yang et al. (2001) reported the *Chandra* ACIS observation of NGC 4151 with notable extended soft X-ray emission on a scale of several hundred parsecs and a spatially unresolved hard X-ray (≥ 2.0 keV) component. The spectrum of the unresolved nuclear source is described by a heavily absorbed ($N_H \sim 10^{22}$ cm^{-2}), hard power-law ($\Gamma \simeq 0.3$) plus soft emission from either a power-law ($\Gamma \simeq 2.6$) or a thermal ($kT \simeq 0.6$ keV) component. We fitted the *XMM-Newton* pn spectrum with a model consisting of a soft component characterized with a power-law plus thermal plasma model with a temperature of $kT \simeq 0.13$ keV and an emission line at 0.88 keV; a hard component characterized with an absorbed power-law ($N_H \simeq 1.8 \times 10^{21}$ cm^{-2}, $\Gamma \simeq 1.75^{+0.06}_{-0.03}$), with warm absorption ($N_H \simeq 5.2^{+1.45}_{-1.20} \times 10^{22}$ cm^{-2}) and partial covering ($N_H \simeq 9.06^{+1.27}_{-0.98} \times 10^{22}$ cm^{-2}, covering fraction $f \simeq 0.69^{+0.04}_{-0.05}$) plus a reflection component and an Fe Kα emission line at 6.4 keV. The Fe Kα line is fitted with a narrow Gaussian component with an EW $\simeq 108.4^{+6.5}_{-6.7}$ eV.

MRK 766

RoSAT and *ASCA* observations showed that the X-ray spectrum of MRK 766 can be described by a power-law of index

~ 1.6 - 2.0 (increasing strongly with flux), a reflection component and a narrow Fe Kα emission line (EW ~ 100 eV) (Leighly et al. 1996). Later observations with *BeppoSAX* found a steeper power-law ($\Gamma \simeq 2.2$) and evidence for an absorption edge at 7.4 keV (Matt et al. 2000b). Using *XMM-Newton* observations Miller et al. (2006) reported the variations in the flux of Fe Kα line on short time scales (5 - 20 ks) and its strong correlation with the continuum emission. We fitted the *XMM-Newton* pn X-ray spectrum of MRK 766 with a less absorbed fairly steep power-law ($\Gamma \simeq 2.17^{+0.10}_{-0.08}$, N_H fixed to Galactic value) with partial covering ($N_H \simeq 6.42^{+0.93}_{-0.56} \times 10^{22}$ cm^{-2}, covering fraction $f \simeq 0.51^{+0.02}_{-0.03}$) and warm absorption ($N_H \simeq 2.1^{+0.28}_{-0.24} \times 10^{21}$ cm^{-2}), a reflection component at the hard end, a soft component fitted with a thermal plasma model of temperature $kT \sim 0.2$ keV and narrow Gaussian emission lines at 0.48 keV, 6.44 keV and 6.67 keV. The Fe Kα emission may have broad component but we get a better fit with a narrow emission line with centroid energy at 6.44 keV and a second narrow line at 6.67 keV. The latter line could be Fe Kα from highly ionized (Fe XXV) material or a K$_\beta$ line from neutral matter.

MRK 231

X-ray observations by ROSAT, *ASCA* (Turner 1999; Iwasawa 1999; Maloney & Reynolds 2000) and more recently *Chandra* (Gallagher et al. 2002; Ptak et al. 2003), have revealed the presence of extended soft X-ray emission of thermal origin that is likely to be associated with the circumnuclear starburst, and a hard and flat ($\Gamma \simeq 0.7$) power-law component as well as an Fe K$_\alpha$ emission line with EW ~ 300 eV (the line was detected by *ASCA* but not by *Chandra*). From combined *XMM-Newton* and *BeppoSAX* observations of MRK 231, Braito et al. (2004) found a highly absorbed ($N_H \sim 2 \times 10^{24}$ cm^{-2}) AGN component. We obtain the best fit with an absorbed power-law ($N_H \simeq 4.6^{+1.4}_{-1.6} \times 10^{21}$ cm^{-2}, $\Gamma \simeq 1.57^{+0.14}_{-0.30}$) accompanied by a partial covering ($N_H \simeq 8.35^{+4.02}_{-4.64} \times 10^{22}$ cm^{-2}, covering fraction $f \simeq 0.74^{+0.09}_{-0.25}$), a soft component fitted with two thermal plasma models with temperatures $kT \simeq 0.33$ keV and 0.99 keV, and narrow emission lines at 6.28 keV and 6.66 keV. The soft X-ray component may have significant contribution from starburst activity (Braito et al. 2004).

ARK 564

Vignali et al. (2004) analyzed two sets of *XMM-Newton* observations of ARK 564 taken a year apart (2000 June and 2001 June) and fitted the 0.6 - 10.0 keV continuum by a soft blackbody component ($kT \simeq 140$ - 150 eV), a steep power-law ($\Gamma \simeq 2.50-2.55$) and an absorption edge at a rest-frame energy of ~ 0.73 keV, corresponding to O VII. No significant spectral changes were observed between the two observations, although the X-ray flux in the second observation is 40 - 50% lower. We obtain the best fit to the 0.6 - 10.0 keV *XMM-Newton* pn spectrum by a less absorbed steep power-law ($\Gamma \simeq 2.32^{+0.08}_{-0.10}$, N_H fixed to the Galactic value) with partial covering ($N_H \simeq 3.09^{+0.52}_{-0.45} \times 10^{22}$ cm^{-2}, covering fraction $f \simeq 0.61^{+0.26}_{-0.15}$), a soft component fitted with a steep power-law ($\Gamma \simeq 3.42^{+0.13}_{-0.12}$), a thermal plasma model with temperature $kT \simeq 0.97$ keV and narrow emission lines at 6.33 keV and 6.71 keV. While fitting we excluded the 0.5 - 0.6 keV part of the spectrum since these data are of poor quality and make it difficult to obtain even a reasonably good fit.

NGC 7469

Blustin et al. (2003) fitted the 0.2 - 10.0 keV *XMM-Newton* EPIC pn spectrum with a combination of a Galactic absorbed power-law ($\Gamma \simeq 1.75$), two blackbody models and a narrow Fe Kα emission line. They noted significant residuals at low energies for which they suggested an instrumental origin. We fitted the 0.5 - 10.0 *XMM-Newton* pn spectrum with a less absorbed power-law ($\Gamma \simeq 2.04^{+0.02}_{-0.02}$, N_H fixed to Galactic value), a partial covering ($N_H \simeq 35.55^{+9.93}_{-6.77} \times 10^{22}$ cm^{-2}, covering fraction $f \simeq 0.28^{+0.03}_{-0.03}$), a soft component fitted with a thermal plasma model of temperature kT $\simeq 0.18$ keV and a narrow Gaussian fitted to the Fe Kα line. Using *ASCA* observations, Reynolds (1997) had reported both narrow and broad components to the Fe line, which was supported by De Rosa et al. (2002) using *BeppoSAX* data, and Nandra et al. (1997) suggested that it was relativistically broadened. We fit the Fe Kα line with a narrow Gaussian component, however, and the data do not need a broad component for a good fit, consistent with Blustin et al. (2003).

MRK 926

Bianchi et al. (2004) fitted the combined 2.5 - 220 keV *XMM-Newton* and *BeppoSAX* spectrum with a baseline model consisting of a power-law ($\Gamma \simeq 1.72^{+0.08}_{-0.06}$) with intrinsic absorption over and above Galactic, a reflection component and a Gaussian to reproduce the Fe Kα line (EW $\simeq 45^{+85}_{-24}$ eV). They also reported an upper limit to the Fe K$_\beta$ flux of the order of the Kα flux, and suggested the possibility of significant contribution from an Fe XXVI line. Weaver et al. (2001) reported strong line variability, both in centroid and in flux, between three *ASCA* observations. We fitted the 0.5 - 10.0 keV *XMM-Newton* spectrum with an absorbed partially covered power-law ($\Gamma \simeq 1.98^{+0.03}_{-0.02}$, N_H fixed to Galactic value, $N_{part,H} \simeq 4.35^{+2.86}_{-1.99} \times 10^{22}$ cm^{-2}, covering fraction $f \simeq 0.15^{+0.06}_{-0.06}$), a reflection component and a narrow Gaussian to fit the Fe Kα line. Notably we do not see any soft excess in this Seyfert.

MRK 530

MRK 530 has not been observed by either *Chandra* or *ASCA*. We present *XMM-Newton* pn spectrum of MRK 530 for the first time. We fitted the 0.5 - 10.0 keV spectrum by an absorbed partially covered power-law ($\Gamma \simeq 2.28^{+0.03}_{-0.01}$, N_H fixed to Galactic value, $N_{part,H} \simeq 14.81^{+5.62}_{-4.18} \times 10^{22}$ cm^{-2}, covering fraction $f \simeq 0.27^{+0.27}_{-0.27}$), a soft component modeled with thermal plasma at a temperature kT $\simeq 0.20$ keV and a narrow Gaussian fitted to the Fe Kα line.

MRK 348

Awaki et al. (2006) fitted the *XMM-Newton* pn 0.2 - 10.0 keV spectrum of MRK 348 with an absorbed power-law ($N_H \simeq 13.5\pm0.02 \times 10^{22}$ cm^{-2}, $\Gamma \simeq 1.61 \pm0.02$), a soft component fitted with a thermal plasma model with temperature kT $\simeq 0.56^{+0.01}_{-0.02}$ keV and an Fe Kα line (EW $\sim 46.4\pm20$ eV), and obtain χ^2/dof ~ 1.46. They fixed the metal abundance of the thermal plasma at 0.1 times the solar abundance, the characteristic value of a normal galaxy (Terashima et al. 2002). We use the same *XMM-Newton* data and find the best fit to the 0.5 - 10.0 keV spectrum consists of an absorbed power-law ($N_H \simeq 6.86^{+0.84}_{-1.01} \times 10^{22}$ cm^{-2}, $\Gamma \simeq 1.70^{+0.07}_{-0.06}$) with partial covering ($N_{H,part} \simeq 10.47^{+0.68}_{-1.00} \times$

10^{22} cm^{-2}, covering fraction $f \simeq 0.84^{+0.06}_{-0.06}$), a soft component fitted with a power-law ($\Gamma \simeq 2.75^{+0.17}_{-0.16}$) and a narrow Gaussian fitted to Fe Kα line (EW $\sim 34.2^{+10.8}_{-10.4}$) and obtained χ^2/dof ~ 1.05.

MRK 1

Guainazzi et al. (2005b) fitted the 0.5 - 10.0 keV *XMM-Newton* pn spectrum of MRK 1 with a highly absorbed power-law ($N_H \geq 110 \times 10^{22}$ cm^{-2}, $\Gamma \simeq 2.41^{+0.13}_{-0.11}$) and a scattered component with partial covering factor fixed to 1, and obtained χ^2/dof $\sim 36/32$. They reported several emission lines including iron K shell lines in 0.5 - 2.0 keV band but no thermal component. In order to constrain the Fe Kα line they performed both global and local fits with centroid energy fixed at 6.4 keV, and found upper limits to the equivalent width of ~ 800 eV and ~ 2.0 keV respectively. Due to the relatively low counts in the data, we use C-statistics to fit the spectrum and find the best fit consists of a hard component (2.0 - 10.0 keV) completely dominated by reflection ($\Gamma \simeq 2.0$), a soft component fitted with a power-law ($\Gamma \simeq 2.55^{+0.30}_{-0.29}$) and a thermal plasma model (kT $\simeq 0.82^{+0.08}_{-0.09}$ keV), and a Gaussian fitted to the Fe Kα line (EW $\sim 1.25^{+1.29}_{-0.86}$ keV). The reflection dominated spectrum, high EW of the Fe line and the low ratio of hard X-ray to [OIII] flux suggest that MRK 1 is likely to be Compton-thick source.

NGC 2273

Guainazzi et al. (2005a) attempted to fit the *XMM-Newton* spectrum of NGC 2273 with a family of models in which hard X-ray component is accounted by an absorbed power-law but yield an unacceptable flat intrinsic spectral index ($\Gamma \simeq -0.2$ - -0.5) and also a large EW ($\simeq 2.0$ - 3.6 keV) of the Fe Kα line with respect to the measured column density ($N_H \simeq 1.4$ - 12.0×10^{22} cm^{-2}), and suggested that the spectrum is dominated by Compton reflection. In the best fit reported by Guainazzi et al. (2005a), the soft X-ray spectrum is accounted by thermal emission model with temperature kT $\simeq 0.8\pm0.2$ keV, hard X-ray fitted by reflection model ($\Gamma_{hard} \simeq 1.5\pm0.4$, $N_H \geq 18.0 \times 10^{23}$ cm^{-2}), and an Fe Kα line with EW $\simeq 2.2^{+0.4}_{-0.3}$ keV. We find the best fit in which hard component is completely accounted by reflection component ($\Gamma \simeq 0.67^{+0.37}_{-0.92}$, PEXRAV model), soft component is fitted with a power-law ($\Gamma \simeq 2.79^{+1.87}_{-0.82}$) and a Gaussian line fitted to Fe Kα (EW $\sim 2.18^{+0.45}_{-0.44}$ keV). Compton-thick nature of this source is evident from the reflection dominated spectrum, high EW of Fe Kα line and low flux ratio of hard X-ray to [OIII].

MRK 78

MRK 78 has not been observed by *Chandra* or *ASCA*. Levenson et al. (2001) fitted its *RoSAT* PSPC soft X-ray spectrum with a thermal plasma (kT $\simeq 0.76$ keV) model absorbed by the Galactic column density and reported extended soft X-ray emission indicative of a circumnuclear starburst. We present the *XMM-Newton* spectrum of MRK 78 for the first time. Our best fit has the hard component completely accounted by a reflection component ($\Gamma \simeq 1.01^{+0.44}_{-0.54}$, 'pexrav' model), the soft component fitted with a very steep power-law ($\Gamma \simeq 7.05^{+1.89}_{-1.84}$), and a Gaussian fitted to Fe Kα (EW ~ 0.67 keV). All the spectral components are absorbed by an equivalent hydrogen column density of $N_H \simeq 6.54^{+3.0}_{-2.5} \times 10^{21}$ cm^{-2}. The predominance of the reflection component, high EW of the Fe Kα line and the ratio of hard X-ray

flux to [OIII] line flux ratio suggest that obscuration is nearly Compton-thick.

NGC 5135

NGC 5135 has not been observed by *XMM-Newton*, and we use the *Chandra* spectral properties given in Guainazzi et al. (2005a) for our study. Both Guainazzi et al. (2005a) and Levenson et al. (2004) obtained substantially similar spectral fits consisting of thermal plus reflection model. The soft X-ray spectrum requires two thermal components with kT $\simeq$ 80 eV and kT $\simeq$ 390 eV plus an additional emission line with centroid energy $E_c \simeq$ 1.78 keV. Above 2.0 keV the spectrum is Compton-reflection dominated, consistent with the AGN being obscured by a column density $N_H \geq 9.0 \times 10^{23}$ cm^{-2} (for an intrinsic photon index of 1.5 and a reflection fraction $\leq$ 0.5). The EW of Fe Kα fluorescent emission line against the reflection continuum is $1.7^{+0.6}_{-0.8}$ keV.
Using *Chandra* observations Levenson et al. (2004) reported a circumnuclear starburst in NGC 5135 and could spatially isolate the AGN emission which is entirely obscured by column density of $N_H \geq 10^{24}$ cm^{-2}, detectable in the *Chandra* bandpass only as a strongly reprocessed weak continuum represented by a flat power-law ($\Gamma \simeq 0$) plus a prominent iron K$_\alpha$ emission line with EW of $\sim$ 2.4 keV. We confirm the Compton-thick obscuration in NGC 5135 using broad-band 0.5 - 50 keV *Suzaku* observations (Singh et al. 2010, in preparation).

MRK 477

MRK 477 has not been observed by *XMM-Newton* or *Chandra*, and we therefore use the *ASCA* spectral properties given in Levenson et al. (2001) for our study. The best fit reported by Levenson et al. (2001) consists of an absorbed power-law ($N_H \simeq 2.4^{+1.7}_{-1.2} \times 10^{23}$ cm^{-2}, $\Gamma \simeq$ 1.9 fixed) and an unresolved Fe Kα emission line of EW $\sim 560^{+560}_{-500}$ eV. The addition of a thermal component kT $\sim$ 0.9 keV to this model renders the reasonable spectral parameter values but did not statistically improve the fit. Heckman et al. (1997) pointed out that MRK 477 has a powerful circumnuclear starburst with the bolometric luminosity of $\sim 3 \times 10^{10}$ - 10^{11} L$_\odot$. This luminosity is comparable to the AGN activity. However, Levenson et al. (2001) concluded that the soft X-ray spectrum is dominated by the AGN.

NGC 5929

NGC 5929 has not been observed by *XMM-Newton* or *Chandra*. Cardamone et al. (2007) have modeled the 0.5 - 8.0 keV *ASCA* spectrum as a sum of three components: a weakly absorbed ($N_{H,1} \simeq 5.16 \times 10^{21}$ cm^{-2}) power-law with photon index $\Gamma \simeq$ 1.70, a heavily absorbed power-law ($N_{H,2} \simeq 2.77 \times 10^{23}$ cm^{-2}) with the same photon index and a Gaussian Fe Kα line of EW of 0.35 keV centered at 6.19 keV. We use the *ASCA* spectral properties of NGC 5929 for our study.

NGC 7212

Guainazzi et al. (2005b) fitted the 0.5 - 10.0 keV *XMM-Newton* spectrum with a heavily absorbed power-law ($N_H \geq 160 \times 10^{22}$ cm^{-2}, $\Gamma \simeq 1.5^{+0.3}_{-0.6}$), two thermal plasma components with kT $\simeq$ 0.16 and 0.72 keV and an Fe Kα line and obtain χ^2/dof $\sim$ 97.0/65. The Fe Kα line was fitted globally as well as locally giving EWs $\sim 900^{+200}_{-300}$ eV and $\sim$ 1100±200 eV, respectively. We fitted the 0.5 - 10.0 keV *XMM-Newton* spectrum with

the hard component completely accounted for by reflection ($\Gamma \simeq 0.99^{+0.54}_{-0.37}$), the soft component fitted with a power-law ($\Gamma \simeq 2.32^{+0.23}_{-0.20}$), a narrow Gaussian fitted to the emission line feature at $\sim$ 0.9 keV and another Gaussian fitted to the Fe Kα emission line at 6.4 keV giving EW $\sim 0.71^{+0.25}_{-0.13}$ keV.

MRK 533

MRK 533 has not been observed by *Chandra* or *ASCA*. Levenson et al. (2001) fitted its ROSAT/PSPC soft X-ray spectrum with a power-law ($\Gamma \simeq 2.0^{+0.7}_{-1.3}$). We present the *XMM-Newton* pn spectrum of MRK 533 for the first time. We fitted the 0.5 - 10.0 keV spectrum with a model in which the soft component is fitted with a power-law ($\Gamma \simeq 3.75^{+1.45}_{-0.61}$) and thermal plasma emission with the temperature kT $\simeq 0.76^{+0.13}_{-0.10}$, a hard component completely accounted for by reflection ($\Gamma \simeq 2.12^{+0.49}_{-0.51}$, PEXRAV model) and narrow Gaussians fitted to the Fe Kα line at 6.4 keV and the Fe K$_\beta$ line at 7.04 keV, with EWs $\sim 0.56^{+0.24}_{-0.29}$ keV and $\sim 0.67^{+0.39}_{-0.33}$ keV, respectively. Our X-ray spectral properties suggest the Compton-thick obscuration in MRK 533.

NGC 7682

We present the *XMM-Newton* spectrum of NGC 7682 for the first time and find the best fit consists of a soft component fitted with a steep power-law ($\Gamma \simeq 5.36^{+2.78}_{-2.38}$), a hard component completely accounted for by reflection ($\Gamma \simeq 1.77^{+0.58}_{-0.61}$, PEXRAV model), and narrow Gaussians fitted to Fe Kα line at 6.4 keV and Fe K$_\beta$ line at 7.11 keV of EWs $\sim 0.48^{+0.31}_{-0.31}$ keV and $\sim 0.46^{+0.46}_{-0.40}$ keV, respectively. All the spectral components are absorbed by an equivalent hydrogen column density $N_H \simeq 3.48^{+5.78}_{-2.51} \times 10^{21}$ cm^{-2}. Our *XMM-Newton* X-ray spectral properties suggest the Compton-thick obscuration in NGC 7682.

References

Akylas, A. & Georgantopoulos, I. 2009, A&A, 500, 999
Antonucci, R. 1993, Annual review of Asto & Asphy, 31, 473
Antonucci, R. 2002, in Astronomical Society of the Pacific Conference Series, Vol. 284, IAU Colloq. 184: AGN Surveys, ed. R. F. Green, E. Y. Khachikian, & D. B. Sanders, 147–+
Antonucci, R. R. J. & Miller, J. S. 1985, ApJ, 297, 621
Arnaud, K. A. 1996, in Astronomical Society of the Pacific Conference Series, Vol. 101, Astronomical Data Analysis Software and Systems V, ed. G. H. Jacoby & J. Barnes, 17–+
Awaki, H., Koyama, K., Inoue, H., & Halpern, J. P. 1991, PASJ, 43, 195
Awaki, H., Murakami, H., Ogawa, Y., & Leighly, K. M. 2006, ApJ, 645, 928
Awaki, H., Terashima, Y., Higaki, Y., & Fukazawa, Y. 2009, PASJ, 61, 317
Awaki, H., Ueno, S., Taniguchi, Y., & Weaver, K. A. 2000, ApJ, 542, 175
Bassani, L., Dadina, M., Maiolino, R., et al. 1999, ApJS, 121, 473
Beckmann, V., Soldi, S., Ricci, C., et al. 2009, A&A, 505, 417
Bianchi, S., Guainazzi, M., Matt, G., et al. 2005a, A&A, 442, 185
Bianchi, S., Matt, G., Balestra, I., Guainazzi, M., & Perola, G. C. 2004, A&A, 422, 65
Bianchi, S., Miniutti, G., Fabian, A. C., & Iwasawa, K. 2005b, MNRAS, 360, 380
Blustin, A. J., Branduardi-Raymont, G., Behar, E., et al. 2003, A&A, 403, 481
Blustin, A. J., Kriss, G. A., Holczer, T., et al. 2007, A&A, 466, 107
Braito, V., Della Ceca, R., Piconcelli, E., et al. 2004, A&A, 420, 79
Buchanan, C. L., Gallimore, J. F., O'Dea, C. P., et al. 2006, AJ, 132, 401
Cappi, M., Panessa, F., Bassani, L., et al. 2006, A&A, 446, 459
Cardamone, C. N., Moran, E. C., & Kay, L. E. 2007, AJ, 134, 1263
Cid Fernandes, R. J., Storchi-Bergmann, T., & Schmitt, H. R. 1998, MNRAS, 297, 579
Dadina, M. 2008, A&A, 485, 417
Dahari, O. & De Robertis, M. M. 1988, ApJ, 331, 727
De Rosa, A., Fabian, A. C., & Piro, L. 2002, MNRAS, 334, L21

Ferruit, P., Wilson, A. S., & Mulchaey, J. 2000, ApJS, 128, 139

Gallagher, S. C., Brandt, W. N., Chartas, G., Garmire, G. P., & Sambruna, R. M. 2002, ApJ, 569, 655

Ghisellini, G., George, I. M., Fabian, A. C., & Done, C. 1991, MNRAS, 248, 14

Ghisellini, G., Haardt, F., & Matt, G. 1994, MNRAS, 267, 743

Gilli, R., Comastri, A., & Hasinger, G. 2007, A&A, 463, 79

González Delgado, R. M., Heckman, T., & Leitherer, C. 2001, ApJ, 546, 845

Grandi, P., Haardt, F., Ghisellini, G., et al. 1998, ApJ, 498, 220

Griffiths, R. G., Warwick, R. S., Georgantopoulos, I., Done, C., & Smith, D. A. 1998, MNRAS, 298, 1159

Guainazzi, M., Fabian, A. C., Iwasawa, K., Matt, G., & Fiore, F. 2005a, MNRAS, 356, 295

Guainazzi, M., Matt, G., & Perola, G. C. 2005b, A&A, 444, 119

Heckman, T. M., Gonzalez-Delgado, R., Leitherer, C., et al. 1997, ApJ, 482, 114

Heckman, T. M., Ptak, A., Hornschemeier, A., & Kauffmann, G. 2005, ApJ, 634, 161

Ho, L. C. & Ulvestad, J. S. 2001, ApJS, 133, 77

Kellermann, K. I., Sramek, R., Schmidt, M., Shaffer, D. B., & Green, R. 1989, AJ, 98, 1195

King, A. 2005, ApJ, 635, L121

Kinkhabwala, A., Sako, M., Behar, E., et al. 2002, ApJ, 575, 732

Krolik, J. H., Madau, P., & Zycki, P. T. 1994, ApJ, 420, L57

Lal, D. V., Shastri, P., & Gabuzda, D. C. 2011, ApJ, 731, 68

Leahy, D. A. & Creighton, J. 1993, MNRAS, 263, 314

Leighly, K. M., Mushotzky, R. F., Yaqoob, T., Kunieda, H., & Edelson, R. 1996, ApJ, 469, 147

Levenson, N. A., Heckman, T. M., Krolik, J. H., Weaver, K. A., & Życki, P. T. 2006, ApJ, 648, 111

Levenson, N. A., Weaver, K. A., & Heckman, T. M. 2001, ApJ, 550, 230

Levenson, N. A., Weaver, K. A., Heckman, T. M., Awaki, H., & Terashima, Y. 2004, ApJ, 602, 135

Magdziarz, P. & Zdziarski, A. A. 1995, MNRAS, 273, 837

Maiolino, R., Ruiz, M., Rieke, G. H., & Papadopoulos, P. 1997, ApJ, 485, 552

Maiolino, R., Salvati, M., Bassani, L., et al. 1998, A&A, 338, 781

Malkan, M. A., Gorjian, V., & Tam, R. 1998, ApJS, 117, 25

Mason, K. O., Branduardi-Raymont, G., Ogle, P. M., et al. 2003, ApJ, 582, 95

Mateos, S., Carrera, F. J., Page, M. J., et al. 2010, A&A, 510, A35+

Matt, G., Bianchi, S., de Rosa, A., Grandi, P., & Perola, G. C. 2006, A&A, 445, 451

Matt, G., Fabian, A. C., Guainazzi, M., et al. 2000a, MNRAS, 318, 173

Matt, G., Fiore, F., Perola, G. C., et al. 1996, MNRAS, 281, L69

Matt, G., Perola, G. C., Fiore, F., et al. 2000b, A&A, 363, 863

Miller, L., Turner, T. J., Reeves, J. N., et al. 2006, A&A, 453, L13

Moran, E. C., Filippenko, A. V., & Kay, L. E. 2000, in Bulletin of the American Astronomical Society, Vol. 32, Bulletin of the American Astronomical Society, 1182–+

Mulchaey, J. S., Koratkar, A., Ward, M. J., et al. 1994, ApJ, 436, 586

Mulchaey, J. S., Wilson, A. S., & Tsvetanov, Z. 1996, ApJ, 467, 197

Nandra, K., George, I. M., Mushotzky, R. F., Turner, T. J., & Yaqoob, T. 1997, ApJ, 477, 602

Nandra, K. & Pounds, K. A. 1994, MNRAS, 268, 405

Nelson, C. H. & Whittle, M. 1995, ApJS, 99, 67

Osterbrock, D. E. & Ferland, G. J. 2006, Astrophysics of gaseous nebulae and active galactic nuclei, ed. Osterbrock, D. E. & Ferland, G. J.

Panessa, F. & Bassani, L. 2002, A&A, 394, 435

Panessa, F., Bassani, L., Cappi, M., et al. 2006, A&A, 455, 173

Perola, G. C., Matt, G., Fiore, F., et al. 2000, A&A, 358, 117

Piro, L., de Rosa, A., Matt, G., & Perola, G. C. 2005, A&A, 441, L13

Polletta, M., Bassani, L., Malaguti, G., Palumbo, G. G. C., & Caroli, E. 1996, ApJS, 106, 399

Pounds, K. A. & Page, K. L. 2005, MNRAS, 360, 1123

Ptak, A., Heckman, T., Levenson, N. A., Weaver, K., & Strickland, D. 2003, ApJ, 592, 782

Reynolds, C. S. 1997, MNRAS, 286, 513

Risaliti, G., Maiolino, R., & Salvati, M. 1999, ApJ, 522, 157

Sako, M., Kahn, S. M., Paerels, F., & Liedahl, D. A. 2000, ApJ, 543, L115

Sambruna, R. M., Netzer, H., Kaspi, S., et al. 2001, ApJ, 546, L13

Schmidt, M. & Green, R. F. 1983, ApJ, 269, 352

Schmitt, H. R., Donley, J. L., Antonucci, R. R. J., Hutchings, J. B., & Kinney, A. L. 2003, ApJS, 148, 327

Schurch, N. J. & Warwick, R. S. 2002, MNRAS, 334, 811

Schurch, N. J., Warwick, R. S., Griffiths, R. E., & Kahn, S. M. 2004, MNRAS, 350, 1

Smith, D. A. & Done, C. 1996, MNRAS, 280, 355

Terashima, Y., Iyomoto, N., Ho, L. C., & Ptak, A. F. 2002, ApJS, 139, 1

Tran, H. D. 2001, ApJ, 554, L19

Tran, H. D. 2003, ApJ, 583, 632

Treister, E., Urry, C. M., & Virani, S. 2009, ApJ, 696, 110

Tueller, J., Mushotzky, R. F., Barthelmy, S., et al. 2008, ApJ, 681, 113

Turner, T. J., George, I. M., Nandra, K., & Mushotzky, R. F. 1997a, ApJS, 113, 23

Turner, T. J., George, I. M., Nandra, K., & Mushotzky, R. F. 1997b, ApJ, 488, 164

Turner, T. J., George, I. M., Nandra, K., & Mushotzky, R. F. 1998, ApJ, 493, 91

Urry, K., Padovanni, G., Wilson, A. S., & Yoshida, M. 1995, ApJ, 521, 565

Vignali, C., Brandt, W. N., Boller, T., Fabian, A. C., & Vaughan, S. 2004, MNRAS, 347, 854

Wang, J., Mao, Y. F., & Wei, J. Y. 2009, AJ, 137, 3388

Weaver, K. A., Gelbord, J., & Yaqoob, T. 2001, ApJ, 550, 261

Weaver, K. A., Nousek, J., Yaqoob, T., et al. 1996, ApJ, 458, 160

Weedman, D. W. 1977, ARA&A, 15, 69

Whittle, M. 1992, ApJS, 79, 49

Worsley, M. A., Fabian, A. C., Bauer, F. E., et al. 2005, MNRAS, 357, 1281

Yang, Y., Wilson, A. S., & Ferruit, P. 2001, ApJ, 563, 124

Yee, H. K. C., Stockman, H. S., & Green, R. F. 1981, in Bulletin of the American Astronomical Society, Vol. 13, Bulletin of the American Astronomical Society, 806–+

Young, A. J., Wilson, A. S., & Shopbell, P. L. 2001, ApJ, 556, 6